J. Marine Sci. Appl. (2011) 10: 265-271
DOI: 10.1007/s11804-011-1068-z

Numerical Simulation of Nonlinear Wave Force on a Quasi-ellipse Caisson

Yongxue Wang*, Xiaozhong Ren and Guoyu Wang

State Key Laboratory of Coastal and Offshore Engineering, Dalian University of Technology, Dalian 116024, China

Abstract: A three dimensional numerical model of nonlinear wave action on a quasi-ellipse caisson in a time domain was developed in this paper. Navier-Stokes equations were solved by the finite difference method, and the volume of fluid (VOF) method was employed to trace the free surface. The partial cell method was used to deal with the irregular boundary typical of this type of problem during first-time wave interaction with the structure, and a satisfactory result was obtained. The numerical model was verified and used to investigate the effects of the relative wave height *H/d*, relative caisson width *kD*, and relative length-width ratio *B/D* on the wave forces of the quasi-ellipse caisson. It was shown that the relative wave height *H/d* has a significant effect on the wave forces of the caisson. Compared with the non-dimensional inline wave force, the relative length-width ratio *B/D* was shown to have significant influence on the non-dimensional transverse wave force.
Keywords: quasi-ellipse caisson; wave force; VOF method; partial cell method
Article ID: 1671-9433(2011)03-0265-07

1 Introduction

The quasi-ellipse caisson is a new type of structure with extensive application prospects for open deepwater wharves. It is made up of three parts; the front and rear parts of the caisson are semicircular sections, and the middle part of the caisson is a rectangular section. The quasi-ellipse caisson is better fitted for a large-scale precast concrete caisson. A wharf structure with one row of quasi-ellipse caissons can effectively avoid differential settlement of the foundation in comparison with the two rows of circular caissons. The gravity dolphin wharf of the quasi-ellipse caisson was first adopted by the Dalian ore terminal phase Ⅱ project (Bai and Hu, 2006). It has helped to significantly reduce the top elevation of the wharf and provide better service functions, safety performance, and economic efficiency (Zhu *et al*., 2007; Dong, 2008).

At present, despite its successful use in practice, little is known about the hydrodynamic behavior of the quasi-ellipse caisson, and few studies have been made on its hydrodynamic characteristics. Experimental investigation of wave force on the quasi-ellipse caisson was carried out by Ren *et al*. (2007, 2009a) and only a relative length-width ratio *B*/*D* of 0.63 was considered. The linear wave force based on the two-dimensional source representation method was also studied by Ren *et al*. (2009b), but the wave forces on the quasi-ellipse caisson predicted by linear wave theory were much smaller than the experimental results for large waves. There is therefore a real need to develop a three dimensional nonlinear numerical model in a time domain as only this approach is capable of dealing with all physical processes involved in the wave-caisson interaction problem.

In this paper, the finite difference method and the volume of fluid (VOF) method, combined with the partial cell method, are used to develop a three dimensional numerical model in a time domain, taking into account the viscosity effect and nonlinear action of waves on structures. By using the VOF method to track the free water surface, the partial cell method is adopted for the first time to deal with the problem of wave interaction with a structure. In this model, the structure shape is accurately described and the conflict between the element number and calculation accuracy is satisfactorily resolved. Then, the numerical model is applied to investigate the effect of the parameters of relative wave height *H*/*d*, relative caisson width *kD*, and relative length-width ratio *B*/*D* on the wave forces of the quasi-ellipse caisson.

2 Numerical model

2.1 Governing equations

The fluid is assumed to be viscous and incompressible, and the fluid motion is governed by the continuity equation and the Navier-Stokes equations. The free surface is traced by the volume of fluid function *F*, where *F* represents the rate of volume in a cell occupied by the fluid to the whole volume of the cell.

$$\frac{\partial}{\partial x}(\theta u)+\frac{\partial}{\partial y}(\theta v)+\frac{\partial}{\partial z}(\theta w)=0 \tag{1}$$

Received date: 2010-09-14.
Foundation item: Supported by the Science and Technology Program on Transportation Construction in Western China, Ministry of Communications under Grant No.2004-328-832-51.
***Corresponding author Email:** wangyx@dlut.edu.cn

$$\frac{\partial u}{\partial t}+u\frac{\partial u}{\partial x}+v\frac{\partial u}{\partial y}+w\frac{\partial u}{\partial z}=-\frac{1}{\rho}\frac{\partial p}{\partial x}+\nu_k\left(\frac{\partial^2 u}{\partial x^2}+\frac{\partial^2 u}{\partial y^2}+\frac{\partial^2 u}{\partial z^2}\right) \quad (2)$$

$$\frac{\partial v}{\partial t}+u\frac{\partial v}{\partial x}+v\frac{\partial v}{\partial y}+w\frac{\partial v}{\partial z}=-\frac{1}{\rho}\frac{\partial p}{\partial y}-g+\nu_k\left(\frac{\partial^2 v}{\partial x^2}+\frac{\partial^2 v}{\partial y^2}+\frac{\partial^2 v}{\partial z^2}\right) \quad (3)$$

$$\frac{\partial w}{\partial t}+u\frac{\partial w}{\partial x}+v\frac{\partial w}{\partial y}+w\frac{\partial w}{\partial z}=-\frac{1}{\rho}\frac{\partial p}{\partial z}+\nu_k\left(\frac{\partial^2 w}{\partial x^2}+\frac{\partial^2 w}{\partial y^2}+\frac{\partial^2 w}{\partial z^2}\right) \quad (4)$$

$$\frac{\partial}{\partial t}(\theta F)+\frac{\partial}{\partial x}(\theta uF)+\frac{\partial}{\partial y}(\theta vF)+\frac{\partial}{\partial z}(\theta wF)=0 \quad (5)$$

In Eqs.(1)–(5), u, v, and w are the velocity components in the x, y, and z directions, respectively. t represents the time, g the gravitational acceleration, ρ the fluid density, p the pressure, ν_k the coefficient of kinematic viscosity, and θ the parameter of partial cell, $\theta\in[0,1]$.

The average value of F in a cell is equal to the fractional volume of the cell occupied by fluid. In particular, a unified value of F corresponds to a cell full with fluid, whereas a zero value indicates that the cell contains no fluid. Cells with F values between zero and one are partially filled with fluid and are either intersected by a free surface or contain voids (bubbles) smaller than the dimensions of the cell mesh. The partial cell method is used to dispose liquid sloshing of any arbitrarily shaped containers in the improved VOF method (Wang and Su, 1991). However, in this paper, the partial cell method is applied to deal with the irregular boundaries of the quasi-ellipse caisson.

2.2 Numerical procedure

2.2.1 Finite difference scheme

A finite difference method is chosen to solve the governing equations. A staggered mesh is used for the computational discretization, as shown in Fig.1. Parameters such as p and F were located at the center of the cell. The velocity component u at the right-hand side of the cell was given as $u_{i+1/2,j,k}$, the vertical velocity v at the top of the cell was written as $v_{i,j+1/2,k}$, and the velocity component w at the front of the cell was written as $w_{i,j,k+1/2}$. Here, $AR_{i,j,k}$, $AT_{i,j,k}$, and $AF_{i,j,k}$ represent the rate of area that can be occupied by the fluid on the right-hand side, top side, and front side, respectively. $VC_{i,j,k}$ indicates the rate of volume in a cell that is occupied by the fluid to the whole volume of the cell. The time derivative is discretized by the forward time difference scheme, and the second-order central difference scheme is applied to discretize the viscosity terms. A combination of the central difference scheme and the upwind scheme is employed to discretize the convection terms.

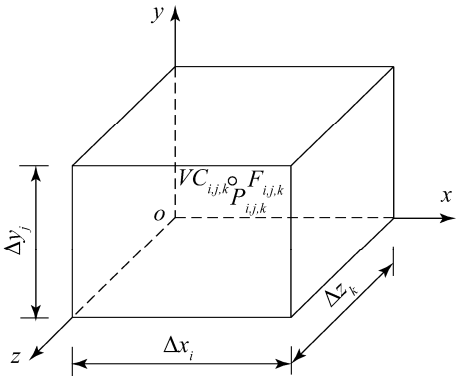

(a) Definition of parameters at the center of the cell

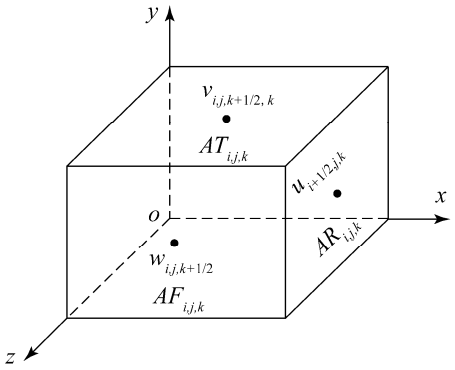

(b) Definition of parameters on the sides of the cell

Fig.1 Sketch of the staggered cell

In this model, the SOLA-VOF algorithm is employed to satisfy the difference equations in each control volume. At each time step the velocity field and pressure in each control volume must be solved. Explicit approximations of the velocity field are obtained from the momentum equations using old time level values. In order to satisfy the continuity equations, the pressure and velocities must be adjusted in each computational cell occupied by fluid. In each cell containing fluid but not a free surface, the cell pressure is adjusted until the continuity equation is satisfied to the required accuracy. For cells containing a free surface, the free surface boundary condition is satisfied by setting the surface cell pressure equal to the value obtained by a linear interpolation between the pressure prescribed at the surface and the pressure of its interpolation cell inside the fluid.

After the velocity field and pressure have been obtained by the above iteration process in each computational cell occupied by fluid, the volume of fluid function F is then computed for the new time level to give the new fluid configuration. The fact that F is a step function requires special care in computing the fluxes to preserve the sharp definition of a free surface; here a donor-acceptor flux approximation of the SOLA-VOF method is used to determine the F function at each interface.

2.2.2 Boundary conditions

The three dimensional numerical wave tank model used in

this study is shown in Fig.2, where L is the tank length, B the tank width, d the water depth, L_1 the length of the working zone of the tank, and L_2 is the length of the velocity reduction zone. The Cartesian coordinate system $oxyz$ is fixed on the tank and the origin is shown in Fig.2.

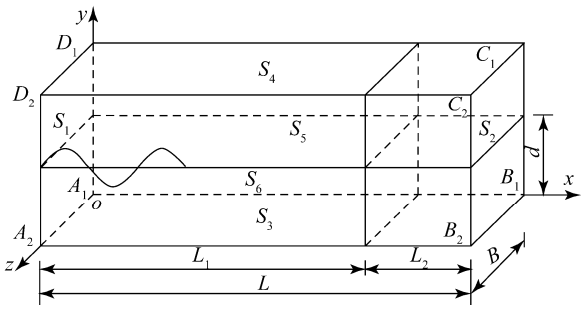

Fig.2 Sketch of 3-D numerical wave tank

The numerical paddles of the wave maker are at the left side of the tank ($S_1 \equiv S_{A_1A_2D_2D_1}$). According to the principle of absorbtion of the wave maker, the paddles are designed to move in a way that generate the required incident waves and at the same time eliminate any reflected wave that reaches them (Wang *et al*., 1999). Based on the Cnoidal wave theory, the paddles' velocity can be expressed as

$$U(k,t)=\eta_0(k,t)c/[d+\eta_0(k,t)]+[\eta_0(k,t)-\eta(k,t)]c/[d+\eta_0(k,t)-\eta(k,t)] \quad (6)$$

where $\eta(k, t)$ is the generated wave surface in front of the kth paddle in the z direction, $\eta_0(k, t)$ the wave surface from the cnoidal theory, d the water depth, and c celerity of the cnoidal wave.

$$\mu(r)=\sqrt{1-\left((r-r_0)/L_2\right)^2} \quad (7)$$

where r_0 is the origin and L_2 is the length of the sponge layers. The reduced vertical velocity inside the sponge layers is obtained by multiplying $\mu(r)$ to the vertical velocity v from the governing equations. Based on the sommerfeld radiation condition, the outflow velocity of the right open boundary is given as:

$$U_{\text{open}}=-\frac{gk\eta}{\omega} \quad (8)$$

where k is the wave number, ω the angular frequency, and η the free surface elevation close to the open boundary.

The boundary of the quasi-ellipse caisson is treated by the partial cell method, which was successfully used to dispose liquid sloshing of any arbitrarily shaped containers in the improved VOF method (Wang and Su, 1991).

Sidewall boundaries ($S_5 \equiv S_{A_1B_1C_1D_1}$ and $S_6 \equiv S_{A_2B_2C_2D_2}$) and the bottom boundary ($S_3 \equiv S_{A_1A_2B_2B_1}$) of the tank are treated as free-slip rigid walls. The normal velocities at the free-slip boundary are set as zero, and the normal derivative of the tangential velocity at the free-slip boundary is zero.

3 Numerical results

3.1 Validation of the numerical wave tank

The properties of the numerical wave tank, such as numerical dissipation, stability, distribution uniformity, and repeatability of waves, are examined first. The wave height H is in the range of 1.0–4.0 m, the wave period T is in the range of 8.0–13.0 s, and the water depth d is 20 m. The total length of the tank is 800 m in which the working zone L_1 is 600 m. The width of the tank is 260 m. The mesh sizes are chosen as Δx =2 m, Δy =3 m, and Δz =2 m. The mean wave heights by an average of five waves at locations $x \approx \lambda, 2\lambda, 3\lambda$, and 4λ (λ being the wave length) along the wave tank are listed in Table 1. The typical time histories of wave surfaces at the location $x \approx 2\lambda$ are shown in Fig.3 and instantaneous wave surfaces in the tank are shown in Fig.4. These figures again clearly confirm that the waves have good uniformity and repeatability.

Table 1 Wave height of different positions in the numerical wave tank

Case	T /s	H /m	d /m	H_λ /m	$H_{2\lambda}$ /m	$H_{3\lambda}$ /m	$H_{4\lambda}$ /m
1	9	1.0	20	1.027	1.005	0.981	0.962
2	10	1.0	20	1.043	1.018	0.998	0.982
3	11	1.0	20	1.021	0.998	0.972	0.942
4	9	1.9	20	1.932	1.890	1.875	1.888
5	10	1.9	20	1.901	1.882	1.875	1.849
6	11	1.9	20	1.903	1.893	1.899	1.897

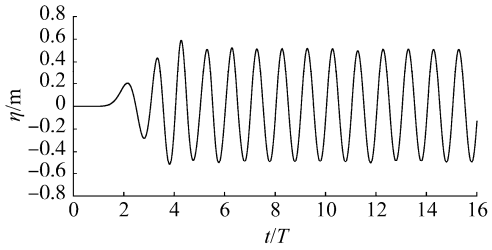

(a) H=1.0 m, T=9.0 s

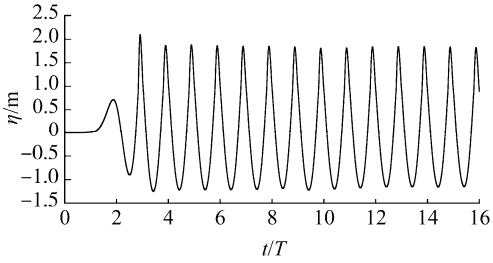

(b) H=3.0 m, T=10.0 s

Fig.3 Time history of wave surface at location x=2 λ

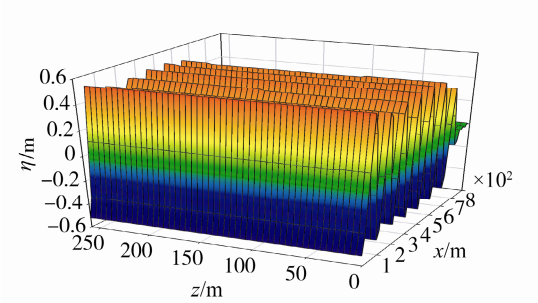

(a) H=1.0 m, T=9.0 s, t=160.0 s

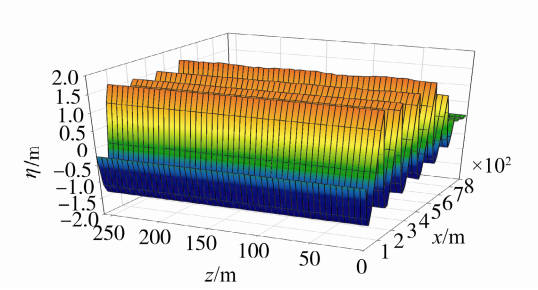

(b) H=3.0 m, T=10.0 s, t=80.0 s

Fig.4 The instantaneous wave surface in the tank

3.2 Verification of the numerical model

The numerical results of the horizontal wave force on the vertical circular cylinder were compared with the results of the analytical solution from the wave diffraction theory (Maccamy *et al*., 1954; Li and Teng, 2002) under weak nonlinear conditions. The wave parameters are chosen as a wave height H=1.9–4.0 m, wave period T=9.0, 12.0 s, and a water depth d=20 m. The radius of the circular cylinder is 10 m. The boundary of the circular cylinder consists of regular obstacle cells and partial cells, as depicted in Fig.5. The plane coordinate of the cell nodes related to the circular cylinder boundary is also shown in Fig.5 and the unit used is meters. It can be seen that the computed wave forces are 7.7% to 13.5% larger than the analytical results from Table 2, and the results reveal that wave nonlinearity became more obvious with an increase in wave height and wave period.

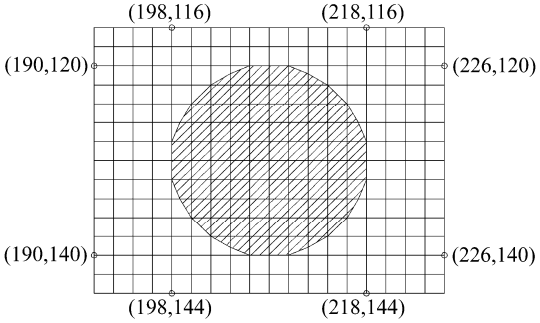

Fig.5 Sketch of the cells on the vertical circular cylinder

Table 2 Comparison of the horizontal wave force on the vertical circular cylinder with the analytical solution

Case	T /s	d /m	H /m	Nonlinear results F_1 /kN	Linear results F_2/kN	ε (%)= $(F_1-F_2)/F_1$
1	9	20.0	1.9	5 059.67	4 670.87	7.7
2	9	20.0	3.0	8 053.73	7 375.06	8.4
3	9	20.0	4.0	10 958.40	9 833.42	10.3
4	12	20.0	1.9	4 466.85	4 062.64	9.0
5	12	20.0	3.0	7 092.71	6 414.70	9.6
6	12	20.0	4.0	9 889.27	8 552.93	13.5

4 Results and discussions

Fig.6 is the sketch of the quasi-ellipse caisson made up of three parts; the front and rear parts of the caisson are the semicircular sections with the diameter D, and the middle part of the caisson is a rectangular section with the length B.

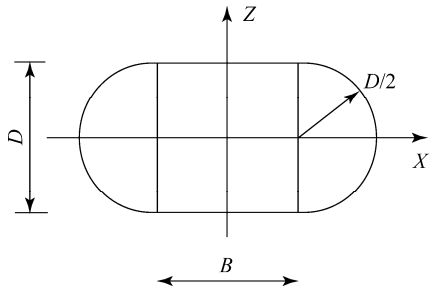

(a) Quasi-ellipse caisson

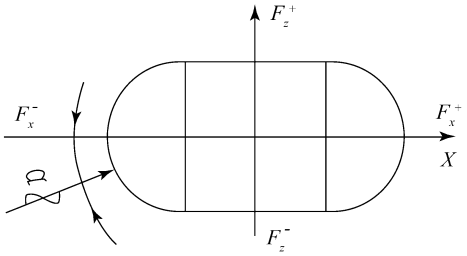

(b) The direction of wave force

Fig.6 Sketch of the quasi-ellipse caisson

The wave parameters are chosen as follows: wave height H=1.0–4.0 m, wave period T=8.0–13.0 s, water depth d=20m. The diameter of the semicircle section D is 20 m. Relative length-width ratio of the quasi-ellipse caisson B/D is arranged from 0 to 0.8, where B represents the length of the rectangular section. Incident wave direction α with 0° and 45° are adopted. Here water density ρ is 1 000 kg/m^3 and gravitational acceleration g is 9.80 m/s^2. The iteration convergence criterion ε with 0.005 is chosen. The boundary of the quasi-ellipse caisson consists of regular obstacle cells and partial cells, as shown in Fig.7. The plane coordinate of cell nodes around the quasi-ellipse caisson is also shown in Fig.7 and the unit is meters. The time step Δt is set to 0.04 s initially and is automatically adjusted to satisfy the Courant condition and a diffusive limit condition.

A numerical simulation is performed to obtain the cnoidal wave forces of the quasi-ellipse caisson. The nondimensional inline wave force $\overline{F_X}$ and the nondimensional transverse wave force $\overline{F_Z}$ are expressed as:

$$\overline{F_X} = F_X / \left\{ \rho g (B+D) d^2 \left[\tanh(kd)/kd \right] \right\} \quad (9)$$

$$\overline{F_Z} = F_Z / \left\{ \rho g (B+D) d^2 \left[\tanh(kd)/kd \right] \right\} \quad (10)$$

where F_X is the inline wave force and is defined as the maximum value of $\left|F_X^+\right|$ and $\left|F_X^-\right|$, and F_Z is the transverse wave force and is defined as the maximum value of $\left|F_Z^+\right|$ and $\left|F_Z^-\right|$, as illustrated in Fig.6. D and $B+D$ are the width and length of the quasi-ellipse caisson, respectively; d is water depth and k is wave number.

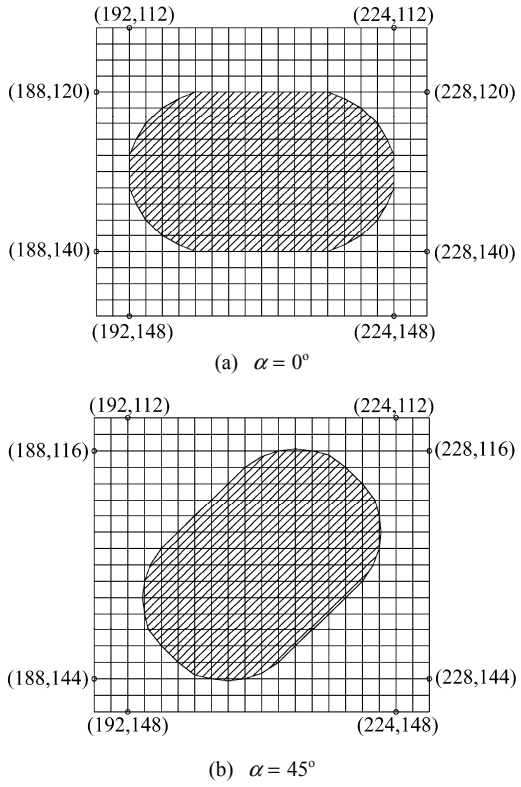

Fig.7 Sketch of the cells on the quasi-ellipse caisson (*B*/*D*=0.6)

The computed wave forces on the quasi-ellipse caisson with the relative length-width ratios 0.2 and 0.6 are compared with linear results based on the two-dimensional source representation method and shown in Fig.8 and in Fig.9, respectively. The relative caisson width *kD* in the range from 0.7 to 1.5 is considered. In the figures, the solid symbols and solid lines represent the computed wave forces, and the hollow symbols and dashed lines indicate the linear results.

The comparison reveals that the computed inline wave force $\overline{F_X}$ and transverse wave force $\overline{F_Z}$ are larger than the linear results. This is due to the time domain numerical model considering the nonlinear effect on wave force of the quasi-ellipse caisson. Relative wave height *H*/*d* has significant effect on the wave forces of the caisson. The larger the relative wave height *H*/*d*, the larger the nondimensional wave forces predicted by the numerical model. Because nonlinear characteristic becomes more obvious with the increase of the relative wave height, the high-order wave force on marine structures becomes more and more obvious; the results reveal that the nonlinear effect on wave force became obvious with the increase of the relative wave height.

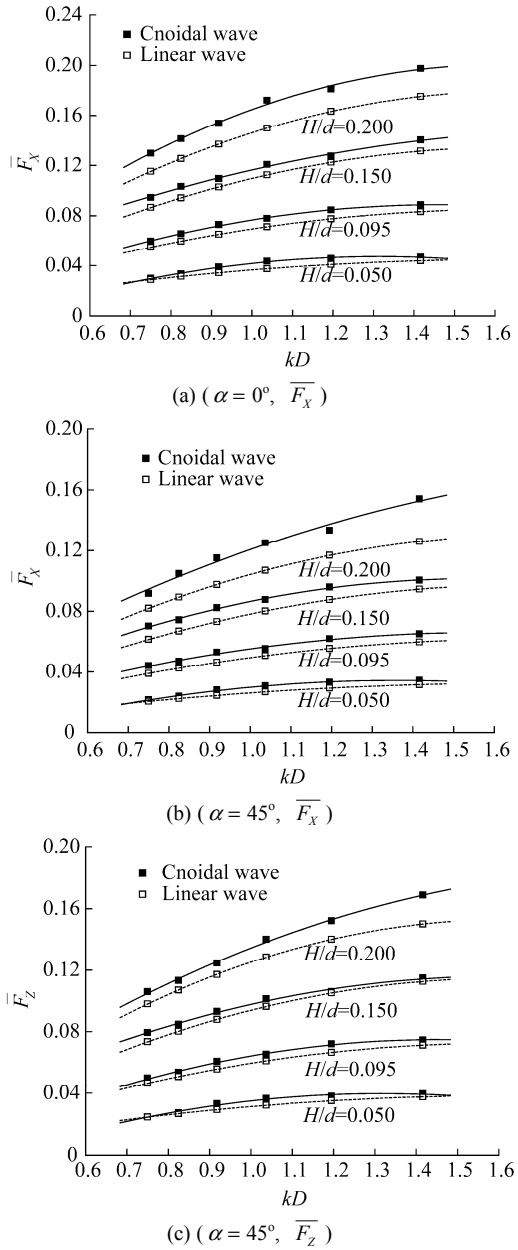

Fig.8 Comparisons of nonlinear and linear wave forces on the quasi-ellipse caisson (*B*/*D*=0.2)

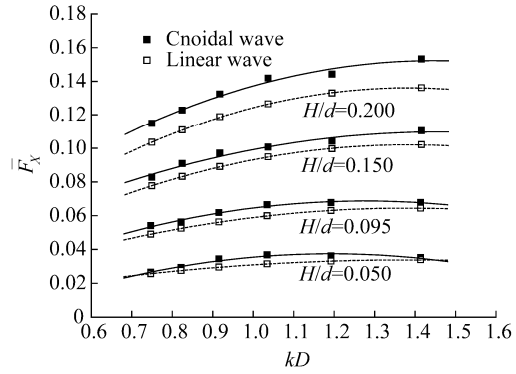

(a) ($\alpha = 0^{o}$, $\overline{F_X}$)

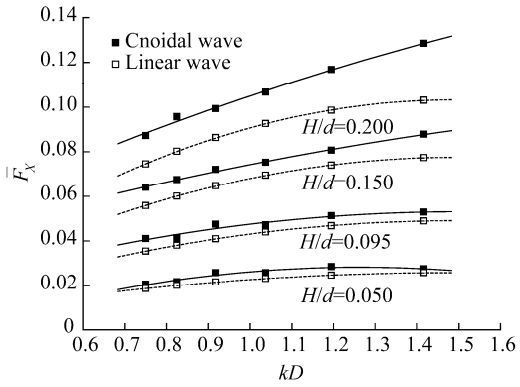

(b) ($\alpha = 45^{o}$, $\overline{F_X}$)

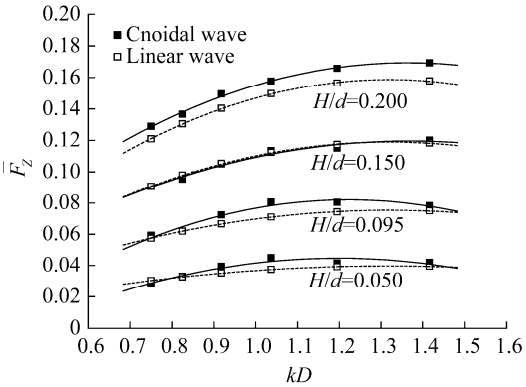

(c) ($\alpha = 45^{o}$, $\overline{F_Z}$)

Fig.9 Comparisons of nonlinear and linear wave forces on the quasi-ellipse caisson (*B*/*D*=0.6)

The nondimensional wave force of a quasi-ellipse caisson at the relative wave height *H*/*d*=0.150 is shown in Fig.10(a) with α=0° and in Fig.10(b) with α=45°. The relative length-width ratio *B*/*D* is arranged from 0.0 to 0.8.

It is shown that the nondimensional wave forces $\overline{F_X}$ and $\overline{F_Z}$ increase with the increase of the relative caisson width *kD*. The nondimensional inline wave force $\overline{F_X}$ decreases with the increase of the relative length-width ratio *B*/*D*, whereas the nondimensional transverse wave force $\overline{F_Z}$ increases as the relative length-width ratio *B*/*D* increases. The larger the relative caisson width *kD*, the more effect the relative length-width ratio *B*/*D* has on the nondimensional inline wave force $\overline{F_X}$. This is due to the ratio of wave length λ with respect to the fact that as caisson length decreases with the increase of the relative wave length *kD*, the effect becomes more obvious. The relative length-width ratio *B*/*D* has much more influence on the nondimensional transverse wave force $\overline{F_Z}$ than the nondimensional inline wave force $\overline{F_X}$.

In Fig.9(b) where α=45°, for the relative length-width ratio *B*/*D* of 0, the quasi-ellipse caisson is a circular caisson, and the nondimensional transverse wave force $\overline{F_Z}$ is equal to the nondimensional inline wave force $\overline{F_X}$. With the increase of the relative length-width ratio *B*/*D*, the nondimensional transverse wave force $\overline{F_Z}$ increases greatly; a main reason for this is that the effective action area of transverse wave force increases quickly with the increase of the relative length-width ratio *B*/*D*. It is seen that the nondimensional transverse wave force $\overline{F_Z}$ is significantly greater than the nondimensional inline wave force $\overline{F_X}$ for the relative length-width ratio *B*/*D* of 0.6 and 0.8.

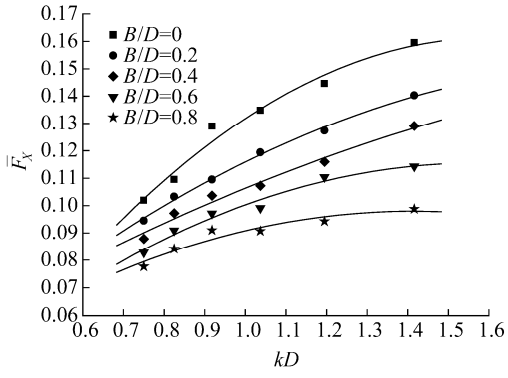

(a) ($\alpha = 0^{o}$, $\overline{F_X}$)

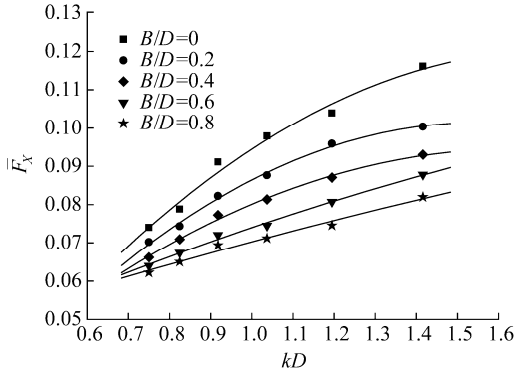

(b) ($\alpha = 45^{o}$, $\overline{F_X}$)

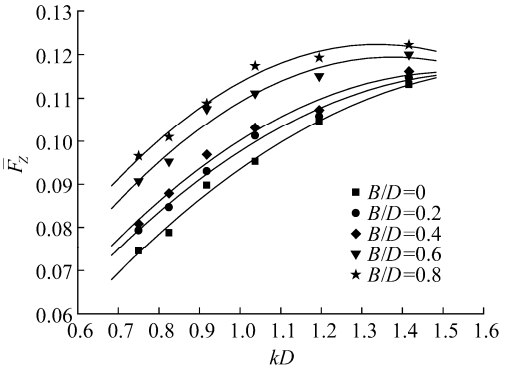

(c) ($\alpha = 45°$, $\overline{F_Z}$)

Fig.10 The nondimensional wave force of the quasi-ellipse caisson versus *kD* at the different relative length-width ratios

5 Conclusions

1) Based on the VOF method and the partial cell method, the three dimensional numerical wave tank model was developed in this paper and used to investigate the nonlinear wave forces of a quasi-ellipse caisson. It was shown that the nonlinear characteristics of the wave forces on quasi-ellipse caissons can be obtained by the numerical model.

2) Relative wave height *H*/*d* has a significant effect on the wave forces of the quasi-ellipse caisson. With the increase of the relative wave height *H*/*d*, the nonlinear characteristics of the wave forces on quasi-ellipse caissons become more important.

3) With the increase of the relative length-width ratio *B*/*D*, the nondimensional inline wave forces decrease and the nondimensional transverse wave forces increase. Compared with the nondimensional inline wave force, the relative length-width ratio *B*/*D* has great influence on the nondimensional transverse wave force. For the relative length-width ratios of 0.6 and 0.8, the nondimensional transverse wave force is significantly greater than the nondimensional inline wave force.

4) The three-dimensional numerical model developed in this paper can be used to simulate the interactions of waves with complex shape structure for engineering applications. Combining with the partial cell method, the model is capable of describing the structure shape accurately and resolving the conflict between the element number and calculation accuracy, thus achieving a good balance between the accuracy and efficiency.

References

Bai Jingtao, Hu Jiashun (2006). Research on and design of new structure of elliptical caissoned pier. *Journal of Port & Waterway Engineering*, **395**(11), 25-30.

Dong Zhongya (2008). Computation method for floating stability of elliptical caissons. *Journal of Port & Waterway Engineering*, **411**(1), 53-59.

Hirt CW, Nichols BD (1981). Volume of fluid (VOF) method for the dynamics of free boundaries. *Journal of Computational Physics*, **39**, 201-225.

Li Yucheng, Teng Bin (2002). *Wave action on maritime structures*. The Ocean Press, Beijing, China, 53-56.

Maccamy RC, Fuchs RA (1954). Wave forces on piles: a diffraction theory. US Army Coastal Engineering Research Center, Tech. Mem., 69.

Qi Peng (2001). *The coupled numerical model for wave actions on structures in the nearshore zone and its applications in engineering*. Ph.D. thesis, Dalian University of Technology, Dalian, 28-29.

Qi Peng, Hou Yijun (2004). A 2D/3D coupled model for wave forces on moored ships in a harbor. *Journal of Hydrodynamics*, *Ser.B*, **16**(5), 633-639.

Ren Xiaozhong, Wang Yongxue, Wang Guoyu (2007). *The wave force on the multiple quasi-ellipse caissons*. *Proceedings of the Fourth International Conference on Asian and Pacific Coasts*, Nanjing, China, 201-208.

Ren Xiaozhong, Wang Yongxue, Wang Guoyu (2009a). Experimental study of wave force on multiple quasi-ellipse caisson structure. *Journal of Dalian University of Technology*, **49**(6), 944-950.

Ren Xiaozhong, Wang Yongxue, Wang Guoyu (2009b). The irregular wave loading on the quasi-ellipse caisson. *Journal of Ship & Ocean Engineering*, **38**(1), 85-89.

Wan Decheng, Miu Guoping (1998). Numerical simulations of waves overtopping an erect quadrate column. *Journal of hydrodynamics*, **13**(3), 363-370.

Wang Yongxue, Su TC (1991). Numerical simulation of liquid sloshing in cylindrical containers. *Acta Aerodyn Sinica*, **9**(1), 112-119.

Wang Yongxue, Zang Jun, Qiu Dahong (1999). Numerical model of cnoidal wave flume. *Journal of China Ocean Engineering*, **13**(4), 391-398.

Zhu Guochun, Ding Jianxin (2007). Design and application of ellipsoidal caisson's suspended rudder. *Journal of China Harbour Engineering*, **150**(4), 61-62.

Yongxue Wang was born in 1955. He is a professor and PhD advisor at Dalian University of Technology. His research interests are nonlinear wave force, wave break-up, wave impact, submarine pipeline spans, and sea ice. He has presided over fifty research subjects.

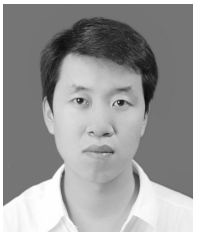

Xiaozhong Ren was born in 1981. He is a PhD candidate at Dalian University of Technology. His research interest is wave interaction with structures.

Guoyu Wang is an associate professor at Dalian University of Technology. His research interests are wave interaction with structures and new breakwaters.